THE JOURNAL OF PHYSICAL CHEMISTRY C

Article

Cite This: J. Phys. Chem. C 2019, 123, 31232−31237

pubs.acs.org/JPCC

Vertical van der Waals Heterostructure of Single Layer InSe and SiGe

I. Eren,[†] S. Ozen,[‡] Y. Sozen,[‡] M. Yagmurcukardes,[*,§] and H. Sahin[‡,∥]

[†]Department of Physics, [‡]Department of Photonics, and [∥]ICTP-ECAR Eurasian Center for Advanced Research, Izmir Institute of Technology, 35430 Izmir, Turkey

[§]Department of Physics, University of Antwerp, Groenenborgerlaan 171, B-2020 Antwerp, Belgium

Supporting Information

ABSTRACT: We present a first-principles investigation on the stability, electronic structure, and mechanical response of ultrathin heterostructures composed of single layers of InSe and SiGe. First, by performing total energy optimization and phonon calculations, we show that single layers of InSe and SiGe can form dynamically stable heterostructures in 12 different stacking types. Valence and conduction band edges of the heterobilayers form a type-I heterojunction having a tiny band gap ranging between 0.09 and 0.48 eV. Calculations on elastic-stiffness tensor reveal that two mechanically soft single layers form a heterostructure which is stiffer than the constituent layers because of relatively strong interlayer interaction. Moreover, phonon analysis shows that the bilayer heterostructure has highly Raman active modes at 205.3 and 43.7 cm^{-1}, stemming from the out-of-plane interlayer mode and layer breathing mode, respectively. Our results show that, as a stable type-I heterojunction, ultrathin heterobilayer of InSe/SiGe holds promise for nanoscale device applications.

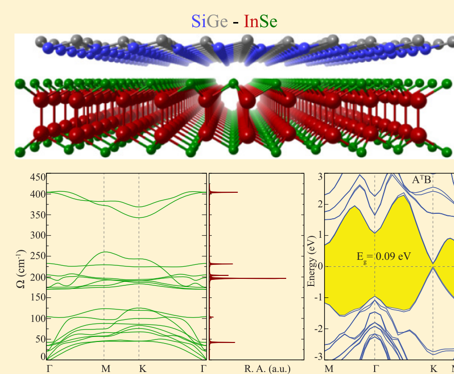

1. INTRODUCTION

Over the last decade, successful isolation of single layer of graphene,[1,2] has attracted great interest toward ultrathin 2D crystals[3−8] and their heterostructures.[9−14] In heterostructures, different types of materials with various characteristic properties are combined in a single structure and therefore, result in novel or enhanced functionalities such as increased quantum efficiency,[15] highly tunable band gap,[16] and high carrier mobilities.[17] Studies performed in a short time have revealed that heterostructures have a great potential for various applications such as photodetectors,[18] valleytronics,[19] and nanoelectronics.[13,20,21] However, search for novel possible heterostructures is still continuing.

Recently synthesized single layer InSe, with its stable ultrathin crystal structure, high electron mobility at room temperature, and semiconducting electronic behavior, is a promising candidate for heterostructure applications.[22,23] It was shown that single layer InSe displays good phototransistor characteristics between the ultraviolet and infrared region.[24,25] It was also reported that single layer InSe can be used as a gas sensor thanks to its surfaces allowing chemical interaction with various gases.[26] Moreover, its strain-tunable electronic band structure[27] and structural stability against large strain application[28] makes single layer InSe a suitable material for electromechanical applications.

Another promising building block for heterostructures is single layer SiGe. In its bulk form, SiGe was reported to be a good candidate for biosensor applications.[29] The experimentally realized SiGe alloy was reported as an appropriate material for solar cell applications.[30] Recent studies have shown that Ge atoms can be incorporated into Si-based nanostructures with negligibly small induced strains.[31,32] The exchange of Si and Ge atoms in Si-based or Ge-based nanostructures may allow the possible experimental realization of the 2D form of SiGe. In addition, the single layer form of SiGe was theoretically predicted to exhibit a dynamically stable[33] buckled structure as a free-standing layer which can be formed upon the incorporation of Si atoms into the germanene layer.[34] It was also shown that halogen-doped SiGe single layers may have a quantum spin hall insulator phase by strain application.[35] Recently, a possible vertical heterostructure of single layers SiGe and h-BN was proposed such that the unique electronic properties of the SiGe layer is preserved in the constructed heterostructure and even a small band gap is created.[36]

In contrast to the metallic substrates, single layer InSe can be a suitable platform for the experimental realization of single layer SiGe. Moreover, the induced biaxial strains on the layer (less than 1.5%) allow the construction of InSe/SiGe heterostructures without any structural changes in the SiGe layer. In this study, the structural, electronic, vibrational, and elastic properties of vertical heterostructures of InSe and SiGe single layers are investigated. It is found that the InSe/SiGe heterostructure forms a dynamically stable type-I heterojunction by conserving the Dirac-cone like electronic nature of the SiGe layer. In addition, the analysis of the Raman spectrum for the heterostructure revealed that the vibrational modes are useful for the investigation of the SiGe structure when

Received: July 5, 2019
Revised: November 14, 2019
Published: December 3, 2019

Downloaded via IZMIR YUKSEK TEKNOLOJI ENSTITUSU on September 6, 2022 at 08:21:07 (UTC).
See https://pubs.acs.org/sharingguidelines for options on how to legitimately share published articles.

ACS Publications © 2019 American Chemical Society

DOI: 10.1021/acs.jpcc.9b06404
J. Phys. Chem. C 2019, 123, 31232−31237

Table 1. For the Single Layer Crystals of InSe and SiGe Structures; the Optimized Lattice Constants (a and b), Atomic Bond Lengths in the Crystals (d_{In-In}, d_{In-Se}, and d_{Si-Ge}), the Amount Charge Depletion of In to In and Se, and Si to Ge (Δ_ρ), SOC Energy Band Gaps Calculated within GGA (E_{gap}^{GGA}) and HSE06 (E_{gap}^{HSE}), Location of VBM and CBM Edges in the BZ, the Work Functions (Φ), Elements of Relaxed-Ion Elastic Stiffness Tensor (C_{ij}), the Corresponding In-Plane Stiffness (C), and Poisson Ratio (ν)

structural phase	a (Å)	b (Å)	d_{In-In}/d_{In-Se} (Å)	d_{Si-Ge} (Å)	Δ_ρIn–In–Se/Si–Ge (e)	E_{gap}^{GGA} (eV)	E_{gap}^{HSE} (eV)	VBM/CBM (—)	Φ (eV)	C_{11} (N/m)	C_{12} (N/m)	C (N/m)	ν (—)
InSe	4.04	4.04	2.79/2.67		0.6	1.61	2.43	$\Gamma-M/\Gamma$	5.70	52	15	48	0.29
SiGe	3.93	3.93		2.35	0.2	0.02	0.08	K/K	4.58/4.50	61	19	55	0.31

synthesized on the InSe layer. Moreover, the in-plane stiffness of the heterostructure indicated quite strong interaction between InSe/SiGe layers.

The paper is organized as follows: details of the computational methodology are given in Section 2. Structural, electronic, vibrational, and elastic properties of single layers of InSe and SiGe are discussed in Section 3. Properties of various stacking types of the InSe/SiGe heterostructure are investigated in Section 4. Finally, we conclude our results in Section 5.

2. COMPUTATIONAL METHODOLOGY

The first-principles calculations within the density functional theory (DFT) were performed for structural optimizations and determination of electronic configurations of InSe and SiGe single layers. In order to model the effect of the core electrons, plane-wave projector-augmented wave potentials[37] were used as implemented in the Vienna Ab initio Simulation Package.[38,39] Using the Perdew–Burke–Ernzerhof form of the generalized gradient approximation (GGA), exchange–correlation energy was described.[40] The electronic band dispersions were calculated within GGA and Heyd–Scuseria–Ernzerhof (HSE06)[41] screened-nonlocal-exchange functional on top of spin–orbit coupling (SOC). Analysis of the charge transfers in the structures was determined by the Bader technique.[42]

The wave functions were expanded up to 500 eV kinetic energy cutoff in the plane-wave basis set.[43] The total energy difference criterion for convergence iterations was 10^{-5} eV, and the force convergence criterion was 10^{-4} eV/Å for the Hellmann–Feynman forces. During the structural calculations, 15 Å vacuum spacing was used to prevent interactions between adjoining cells, and the Becke–Johnson damping of the DFT-D3 method was used to implement the van der Waals (vdW) corrections.[43] In addition, a Γ-centered 36 × 36 × 1 k-point mesh was used for the accurate density of states calculations and the density of states patterns are obtained by using 0.05σ values for Gaussian broadening. Phonon band dispersions were calculated by using the small displacement method as implemented in the PHON code.[44]

The layer–layer interaction energy was calculated by using the formula: $E_{int} = E_{InSe} + E_{SiGe} - E_{het}$, where E_{InSe}, E_{SiGe}, and E_{het} stands for the ground state energies of single layer InSe, SiGe, and InSe/SiGe heterostructure, respectively.

3. 2D SINGLE LAYERS OF INSE AND SIGE

The optimized lattice parameters, $a = b$, of the two single layers are calculated to be 4.04 and 3.93 Å for InSe and SiGe single layers, respectively. The corresponding atomic bond lengths are listed in Table 1. The Bader charge analysis reveals that the In–Se crystal structure is formed by donation of 0.6 e from the In atom to the Se atom indicating the mostly ionic character of the bonds. On the other hand, in single layer SiGe crystal covalent bonds formed with depletion of 0.2 e from the Si to Ge atom. In addition, the thermionic work function (Φ) of each single layer are calculated to be 5.70 eV for InSe and 4.58/4.50 eV for SiGe calculated from Si–Ge surfaces, respectively. Calculated phonon spectra shown in Figure 1b, confirms that both of the single layer crystals are dynamically stable structures. Monolayer InSe exhibits five Raman active phonon modes (three doubly-degenerate in-plane and two nondegenerate out-of-plane). The in-plane vibrational phonon

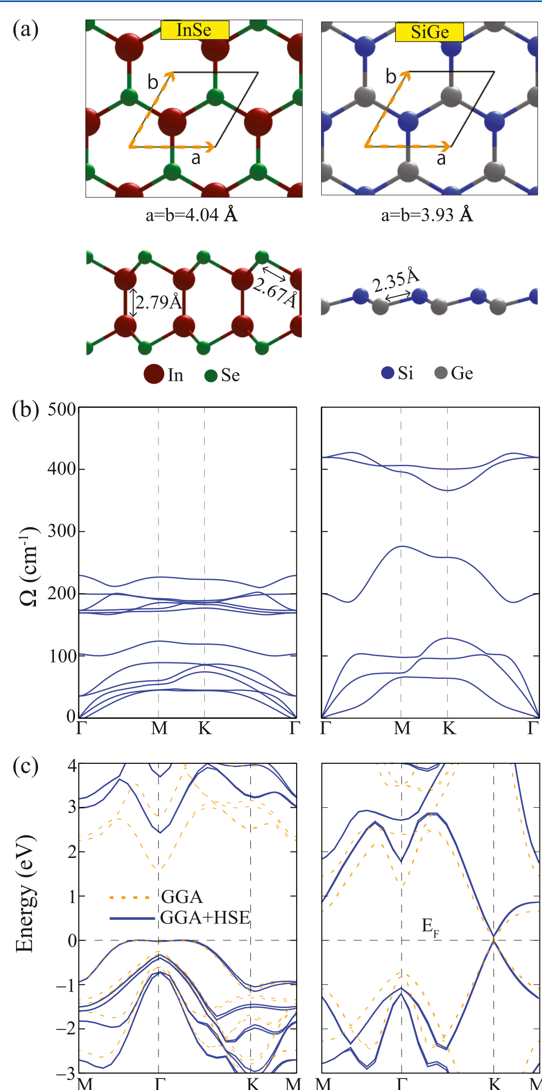

Figure 1. For the single layers of InSe (left panel) and SiGe (right panel); (a) top and side views of the crystal structures, (b) corresponding phonon band dispersions, and (c) SOC-included electronic band structures calculated within GGA and HSE06, respectively. The Fermi level is set to zero.

DOI: 10.1021/acs.jpcc.9b06404
J. Phys. Chem. C 2019, 123, 31232–31237

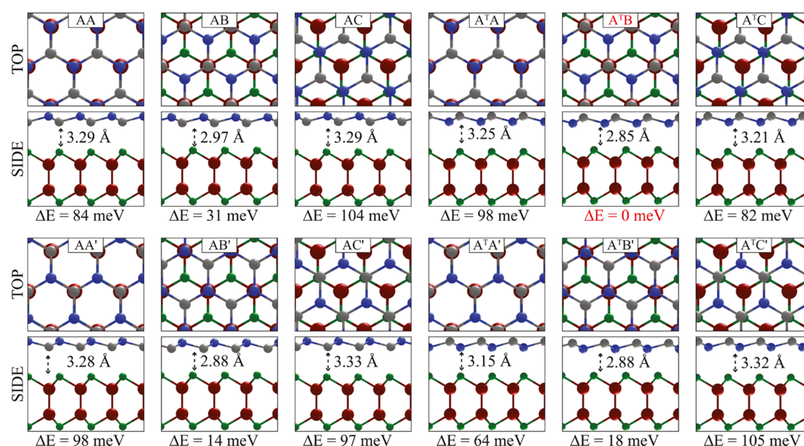

Figure 2. Top and side views of various stacking configurations for InSe/SiGe heterostructures. The total energy differences with respect to the ground state stacking and the layer−layer distances are also given.

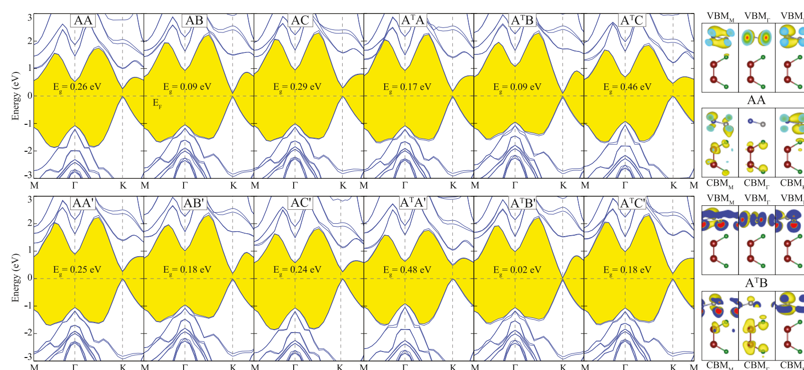

Figure 3. Electronic band structures of 12 stacking orders calculated using HSE06. The band-decomposed charge densities at three different high-symmetry points for two different stackings are shown on the right panel. The Fermi level is set to zero.

modes (E^2_{1g}, E^1_{1g}, and E^1_{2g}) have frequencies 35.6, 169.2, and 173.2 cm^{-1} at the Γ point, respectively. Moreover, the out-of-plane Raman active modes (A^2_{1g} and A^1_{1g}) are found to have frequencies 103.3 and 229.4 cm^{-1} at the Γ point, respectively. The SiGe single layer have 2 Raman active phonon modes, one out-of-plane, A-peak (199.7 cm^{-1}), and a doubly-degenerate in-plane mode, E-peak (417.0 cm^{-1}).

Electronic band dispersions of single layers of InSe and SiGe are presented in Figure 1c. It has been demonstrated experimentally that single layer InSe exhibits an indirect band gap of ∼2.9 eV.[45] Our results reveal that the valence band edge between the M and the Γ points has slightly larger energy than that of at the Γ point. Thus, single layer InSe is found to be an indirect band gap semiconductor with the valence band maximum (VBM) and the conduction band minimum (CBM) residing at the M−Γ and Γ points of the Brilouin Zone (BZ), respectively. The calculated band gap is 2.43 eV which is slightly underestimated by our methodology. On the other hand, single layer SiGe possesses a direct band gap semiconducting nature with a band gap of 0.08 eV with VBM and CBM residing at the K point. The p-orbitals of In and Se atoms significantly contribute to the VBM while the In-s and the Se-p orbitals are dominant at CBM for single layer InSe. In single layer SiGe, the Si-p and Ge-p orbitals are significantly effective at the Fermi level.

The elastic properties of single layers of InSe and SiGe are analyzed in terms of the two independent constants: in-plane stiffness, C, and Poisson ratio, ν. In order to determine the linear-elastic constants, the C and ν values are calculated by using the elastic strain tensor elements as $C = \frac{C_{11}^2 - C_{12}^2}{C_{11}}$ and $\nu = C_{12}/C_{11}$. Note that, because of the in-plane isotropic nature of the single layers, both of the elastic constants are the same and independent of the orientation of the lattice. As listed in Table 1, single layer SiGe is found to be slightly stiffer than single layer InSe (55 and 48 N/m, respectively). Apparently, compared to its parents, single layer InSe is softer than single layers GaS and GaSe (91 and 77 N/m, respectively).[46] On the other hand, the in-plane stiffness of single layer SiGe is calculated to be larger than that of germanene (48 N/m) and smaller than that of silicene (62 N/m) as expected.[33] However, as compared to other well-known 2D single layers such as graphene (330 N/m) and MoS_2 (122 N/m),[46] both single layers of InSe and SiGe are softer materials. Moreover, the Poisson ratio which is the ratio of the transverse contraction strain to the longitudinal extension, is calculated to be 0.29 for single layer InSe which is quite close to that of single layers GaS (0.29) and GaSe (0.30).[46] However, the Poisson ratio of single layer SiGe is calculated to be 0.31 which is larger than that of single layer MoS_2 (0.26)[46] and in between that of silicene (0.30) and germanene (0.33).[33]

4. POSSIBLE VERTICAL HETEROSTRUCTURES OF INSE AND SIGE

As shown in Figure 2, InSe and SiGe single layers can be vertically combined to construct a bilayer heterostructure in 12

DOI: 10.1021/acs.jpcc.9b06404
J. Phys. Chem. C 2019, 123, 31232−31237

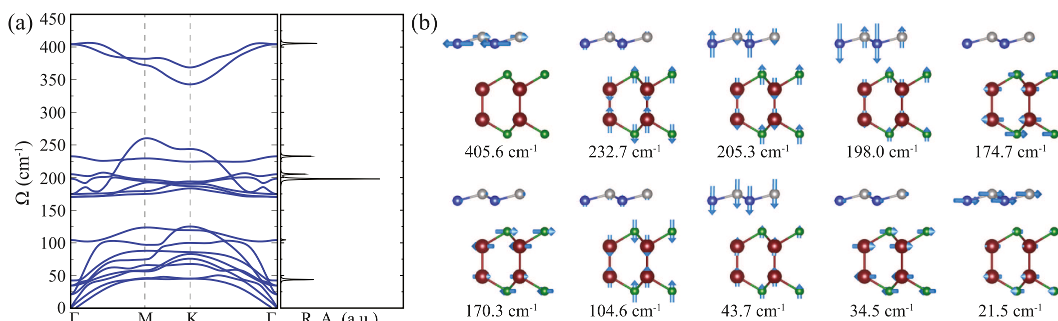

Figure 4. For the ground state stacking of InSe/SiGe heterostructure; (a) phonon-band dispersion (left panel), and corresponding Raman activities (right panel) in arbitrary units. (b) Vibrational characteristics of Raman active phonon modes. The frequency of each mode is given below.

different stacking types. The 12 stacking types are classified such that for the 6 stackings (AA, AB, AC, AA′, AB′, and AC′) the Ge atoms reside closer to the InSe layer while for the remaining 6 stacking orders (A^TA, A^TB, A^TC, A^TA', A^TB', and A^TC') Si atoms form the intimate contact layer. The total energy calculations reveal that the A^TB is the ground state stacking order with the shortest layer−layer distance (2.85 Å). The total energy differences are found to vary from 14 to 105 meV per unit cell and heterostructure. In addition, the calculated layer−layer interaction energies (ranging from 34 to 52 meV/atom) indicate slightly strong interaction between InSe and SiGe layers [relatively higher than MoS_2/WS_2 (33 meV/atom)][47] that can be related to the reactive nature of the buckled SiGe layer. As reported previously, the strong interaction between germanene and InSe layers results in orbital hybridization between upper Se atoms of InSe and lower Ge atoms of germanene layers.[48] Regardless of the stacking type in the heterostructure, the optimized lattice parameters are calculated to be $a = b = 3.98$ Å which indicates that the varying interlayer distance is not sufficiently large in order to change the induced biaxial strains on the layers. Thus, an amount of 1.5% compressive strain occurs on the InSe layer while the SiGe layer is under a tensile strain of 1.3%.

The electronic properties of each stacking type are obtained in terms of their electronic band dispersions (see Figure 3). It is clear that all stacking types are found to form type-I heterojunction whose VBM and CBM are primarily composed of the Si and Ge states. This type of band alignment allows for the confinement of electrons and holes which is useful in optoelectronic applications such as solar cells. Therefore, type-I band alignment of InSe/SiGe is a possible candidate for such applications. The electronic nature of the SiGe layer is preserved in the heterostructure; however, its tiny direct band gap is found to vary from 0.02 eV (in A^TB' stacking) to 0.48 eV (in A^TA' stacking). The variation of the electronic band gap is related to the induced biaxial strains on the layers and to the layer−layer interaction. Because the effect of the induced strain remains the same in all stacking types, evidently the variation of the band gap is dominated by the interlayer interaction. As seen from the band-decomposed charge densities (shown on the right panel of Figure 3) plotted for two different stacking types, the variation of the interlayer distance affects the orbital hybridization between upper Se and lower Si or Ge atoms. Moreover, it is evident that the valence band edges at the 3 high symmetry points (M, Γ, and K) are composed of Si- and Ge-orbitals while In- and Se-orbitals only contribute to the conduction band edges at the M and the Γ points.

In order to discuss the general phononic behavior and dynamical stability of the InSe/SiGe heterostructure, we present a detailed investigation on the lowest energy stacking A^TB. As shown in Figure 4a, the phonon dispersion is free from any imaginary frequencies through the whole BZ indicating the dynamical stability of the structure. At the Γ point there are three phonon modes having frequencies 21.5, 34.5, and 43.7 cm^{-1} in the low-frequency regime. The modes at 21.5 and 43.7 cm^{-1} are assigned as the in-plane shear mode (SM) and the out-of-plane layer breathing (LBM), respectively. On the other hand, the phonon mode having frequency 34.5 cm^{-1} arises completely from the InSe layer that the upper and lower In−Se pairs vibrate against each other (see Figure 4b). Among the low-frequency modes, especially the LBM, with its high Raman activity, directly shows the formation of the heterostructure and it can be observed experimentally. In addition, the low-frequency phonon modes give direct information about the layer−layer interaction in the heterostructure.

In the high frequency regime (between ∼100 and 450 cm^{-1}) there are three doubly degenerate in-plane and four non-degenerate out-of-plane vibrational modes. The phonon modes at 104.6, 170.3, and 174.7 cm^{-1} simply arise from the InSe layer. The mode at 104.6 cm^{-1} is attributed to the out-of-plane vibration of sub-InSe pairs. In addition, the most prominent phonon peaks appear at 198.0 and 205.3 cm^{-1}. In these modes, although both of them have the same optical out-of-plane character in individual layers, difference in the eigenfrequency simply arise from whether the intimate contact atoms are in-phase or out-of-phase. In addition, the out-of-plane vibrational mode at 232.7 cm^{-1}, having almost no dispersion through the whole Brillouin zone, is composed of the out-of-phase vibrations of sub-InSe layers. The highest frequency mode at 405.6 cm^{-1} simply stem from the LO−TO phonons which are degenerate at the Γ point.

For the ground state stacking configuration, the elastic coefficients and the corresponding elastic parameters are also calculated. The in-plane stiffness of a heterostructure is smaller than the sum of those of the individual layers because of the loss driven by the weak vdW interaction between the layers.[49] Here, the in-plane stiffness of the heterostructure is calculated using the equation; $C_{hetero} = C_{InSe} + \alpha C_{SiGe}$ where C_{hetero}, C_{InSe}, and C_{SiGe} are the in-plane stiffness of the heterostructure, InSe, and SiGe layer, respectively, while α is the interaction coefficient ranging from 0 to 1. Therefore, the in-plane stiffness of heterobilayer C_{hetero} is calculated to be 98 N/m which is slightly smaller than the sum of in-plane stiffness of the individual layers (103 N/m). It appears that the interaction coefficient, α, is found to be 0.91 which is larger than that

DOI: 10.1021/acs.jpcc.9b06404
J. Phys. Chem. C 2019, 123, 31232−31237

measured for the MoS_2/WS_2 heterostructure (0.80), for bilayer MoS_2 (0.75), and for the MoS_2/graphene heterostructure (0.69).[49] It can be also inferred from the α value that the contribution of the SiGe layer to the in-plane stiffness is sufficiently large. In addition, the Poisson ratio of the heterostructure is calculated to be 0.31 which is in between those for the individual layers. This can be related the weak in-plane component of the interlayer forces between the layers.

5. CONCLUSIONS

In this study, we investigated the formation, stability, electronic properties, phononic characteristics, and mechanical response of bilayer heterostructure InSe/SiGe by means of state-of-the-art first-principles calculations. It was found that (i) two single layers form a dynamically stable type-I vertical heterojunction with an electronic band gap (ranges between 0.09 and 0.48 eV) sensitive to the stacking configuration, (ii) highly Raman active phonon mode at 43.7 cm^{-1}, indicating the formation of the heterostructure directly and can be observed by experimental tools, and (iii) the in-plane stiffness of the heterostructure is slightly smaller than the sum of the individual stiffnesses indicating relatively strong interaction of the layers. The heterobilayer of InSe/SiGe, with its dynamically stable atomic structure and electronic behavior forming a type-I hetero-junction, is a potential candidate for nanoscale optoelectronic device applications.

■ ASSOCIATED CONTENT

Supporting Information

The Supporting Information is available free of charge at https://pubs.acs.org/doi/10.1021/acs.jpcc.9b06404.

Calculated band dispersion, interlayer distance dependent band dispersion, and optimized geometries (PDF)

■ AUTHOR INFORMATION

Corresponding Author

*E-mail: mehmetyagmurcukardes.edu@gmail.com.

ORCID

M. Yagmurcukardes: 0000-0002-1416-7990

H. Sahin: 0000-0002-6189-6707

Notes

The authors declare no competing financial interest.

■ ACKNOWLEDGMENTS

Computational resources were provided by TUBITAK ULAKBIM, High Performance and Grid Computing Center (TR-Grid e-Infrastructure) and by Flemish Supercomputer Center (VSC). H.S. acknowledges financial support from the TUBITAK under project number 117F095. H.S. acknowledges support from the Turkish Academy of Sciences under the GEBIP program. This work is supported by the Flemish Science Foundation (FWO-Vl) by a postdoctoral fellowship (M.Y.).

■ REFERENCES

(1) Novoselov, K. S.; Geim, A. K.; Morozov, S. V.; Jiang, D.; Zhang, Y.; Dubonos, S. V.; Grigorieva, I. V.; Firsov, A. A. Electric Field Effect in Atomically Thin Carbon Films. *Science* **2004**, *306*, 666−669.

(2) Geim, A. K.; Novoselov, K. S. The rise of graphene. *Nat. Mater.* **2007**, *6*, 183−191.

(3) Mak, K. F.; Lee, C.; Hone, J.; Shan, J.; Heinz, T. F. Atomically Thin MoS_2: A New Direct-Gap Semiconductor. *Phys. Rev. Lett.* **2010**, *105*, 136805.

(4) Splendiani, A.; Sun, L.; Zhang, Y.; Li, T.; Kim, J.; Chim, C.-Y.; Galli, G.; Wang, F. Emerging Photoluminescence in Monolayer MoS_2. *Nano Lett.* **2010**, *10*, 1271−1275.

(5) Radisavljevic, B.; Radenovic, A.; Brivio, J.; Giacometti, V.; Kis, A. Single-layer MoS_2 transistors. *Nat. Nanotechnol.* **2011**, *6*, 147−150.

(6) Zhang, Y.; Chang, T. R.; Zhou, B.; Cui, Y. T.; Yan, H.; Liu, Z.; Schmitt, F.; Lee, J.; Moore, R.; Chen, Y.; Lin, H.; Jeng, H. T.; Mo, S. K.; Hussain, Z.; Bansil, A.; Shen, Z. X. Direct observation of the transition from indirect to direct bandgap in atomically thin epitaxial $MoSe_2$. *Nat. Nanotechnol.* **2014**, *9*, 111−115.

(7) Zhao, W.; Ghorannevis, Z.; Chu, L.; Toh, M.; Kloc, C.; Tan, P.-H.; Eda, G. Evolution of Electronic Structure in Atomically Thin Sheets of WS_2 and WSe_2. *ACS Nano* **2013**, *7*, 791−797.

(8) Tongay, S.; Sahin, H.; Ko, C.; Luce, A.; Fan, W.; Liu, K.; Zhou, J.; Huang, Y.-S.; Ho, C.-H.; Yan, J.; Ogletree, D. F.; Aloni, S.; Ji, J.; Li, S.; Li, J.; Peeters, F. M.; Wu, J. Monolayer behaviour in bulk ReS_2 due to electronic and vibrational decoupling. *Nat. Commun.* **2014**, *5*, 3252.

(9) Jariwala, D.; Sangwan, V. K.; Lauhon, L. J.; Marks, T. J.; Hersam, M. C. Emerging Device Applications for Semiconducting Two-Dimensional Transition Metal Dichalcogenides. *ACS Nano* **2014**, *8*, 1102−1120.

(10) Novoselov, K. S.; Mishchenko, A.; Carvalho, A.; Castro Neto, A. H. 2D materials and van der Waals heterostructures. *Science* **2016**, *353*, aac9439.

(11) Withers, F.; Del Pozo-Zamudio, O.; Mishchenko, A.; Rooney, A. P.; Gholinia, A.; Watanabe, K.; Taniguchi, T.; Haigh, S. J.; Geim, A. K.; Tartakovskii, A. I.; Novoselov, K. S. Light-emitting diodes by band-structure engineering in van der Waals heterostructures. *Nat. Mater.* **2015**, *14*, 301−306.

(12) Jariwala, D.; Marks, T. J.; Hersam, M. C. Mixed-dimensional van der Waals heterostructures. *Nat. Mater.* **2017**, *16*, 170−181.

(13) Rivera, P.; Schaibley, J. R.; Jones, A. M.; Ross, J. S.; Wu, S.; Aivazian, G.; Klement, P.; Seyler, K.; Clark, G.; Ghimire, N. J.; Yan, J.; Mandrus, D. G.; Yao, W.; Xu, X. Observation of long-lived interlayer excitons in single layer $MoSe_2WSe_2$ heterostructures. *Nat. Commun.* **2015**, *6*, 6242.

(14) Deng, D.; Novoselov, K. S.; Fu, Q.; Zheng, N.; Tian, Z.; Bao, X. Catalysis with two-dimensional materials and their heterostructures. *Nat. Nanotechnol.* **2016**, *11*, 218−230.

(15) Gong, Y.; Lei, S.; Ye, G.; Li, B.; He, Y.; Keyshar, K.; Zhang, X.; Wang, Q.; Lou, J.; Liu, Z.; Vajtai, R.; Zhou, W.; Ajayan, P. M. Two-Step Growth of Two-Dimensional $WSe_2/MoSe_2$ Heterostructures. *Nano Lett.* **2015**, *15*, 6135−6141.

(16) Yagmurcukardes, M.; Torun, E.; Senger, R. T.; Peeters, F. M.; Sahin, H. $Mg(OH)_2WS_2$ van der Waals heterobilayer: Electric field tunable band-gap crossover. *Phys. Rev. B* **2016**, *94*, 195403.

(17) Jin, H.; Li, J.; Wang, B.; Yu, Y.; Wan, L.; Xu, F.; Dai, Y.; Wei, Y.; Guo, H. Electronics and optoelectronics of lateral heterostructures within monolayer indium monochalcogenides. *J. Mater. Chem. C* **2016**, *4*, 11253−11260.

(18) Barati, F.; Grossnickle, M.; Su, S.; Lake, R. K.; Aji, V.; Gabor, N. M. Hot carrier-enhanced interlayer electron-hole pair multiplication in 2D semiconductor heterostructure photocells. *Nat. Nanotechnol.* **2017**, *12*, 1134−1139.

(19) Hanbicki, A. T.; Chuang, H.-J.; Rosenberger, M. R.; Hellberg, C. S.; Sivaram, S. V.; McCreary, K. M.; Mazin, I. I.; Jonker, B. T. Double Indirect Interlayer Exciton in a $MoSe_2/WSe_2$ van der Waals Heterostructure. *ACS Nano* **2018**, *12*, 4719−4726.

(20) Tang, H.-L.; Chiu, M.-H.; Tseng, C.-C.; Yang, S.-H.; Hou, K.-J.; Wei, S.-Y.; Huang, J.-K.; Lin, Y.-F.; Lien, C.-H.; Li, L.-J. Multilayer $GrapheneWSe_2$ Heterostructures for WSe_2 Transistors. *ACS Nano* **2017**, *11*, 12817−12823.

(21) Qiao, H.; Yuan, J.; Xu, Z.; Chen, C.; Lin, S.; Wang, Y.; Song, J.; Liu, Y.; Khan, Q.; Hoh, H. Y.; Pan, C.-X.; Li, S.; Bao, Q. Broadband Photodetectors Based on $GrapheneBi_2Te_3$ Heterostructure. *ACS Nano* **2015**, *9*, 1886−1894.

(22) Brotons-Gisbert, M.; Andres-Penares, D.; Suh, J.; Hidalgo, F.; Abargues, R.; Rodríguez-Cantó, P. J.; Segura, A.; Tobias, G.; Canadell, E.; Ordejón, P.; Wu, J.; Martínez-Pastor, J. P.; Sánchez-Royo, J. F.; Sánchez-Royo, J. F. Nanotexturing To Enhance Photoluminescent Response of Atomically Thin Indium Selenide with Highly Tunable Band Gap. *Nano Lett.* **2016**, *16*, 3221−3229.

(23) Bandurin, D. A.; Tyurina, A. V.; Yu, G. L.; Mishchenko, A.; Zólyomi, V.; Morozov, S. V.; Kumar, R. K.; Gorbachev, R. V.; Kudrynskyi, Z. R.; Pezzini, S.; Kovalyuk, Z. D.; Zeitler, U.; Novoselov, K. S.; Patané, A.; Eaves, L.; Grigorieva, I. V.; Falko, V. I.; Geim, A. K.; Cao, Y. High electron mobility, quantum Hall effect and anomalous optical response in atomically thin InSe. *Nat. Nanotechnol.* **2017**, *12*, 223−227.

(24) Yang, Z.; Jie, W.; Mak, C.-H.; Lin, S.; Lin, H.; Yang, X.; Yan, F.; Lau, S. P.; Hao, J. Wafer-Scale Synthesis of High-Quality Semiconducting Two-Dimensional Layered InSe with Broadband Photoresponse. *ACS Nano* **2017**, *11*, 4225−4236.

(25) Lei, S.; Wen, F.; Ge, L.; Najmaei, S.; George, A.; Gong, Y.; Gao, W.; Jin, Z.; Li, B.; Lou, J.; Kono, J.; Vajtai, R.; Ajayan, P.; Halas, N. J. An Atomically Layered InSe Avalanche Photodetector. *Nano Lett.* **2015**, *15*, 3048−3055.

(26) Cai, Y.; Zhang, G.; Zhang, Y.-W. Charge Transfer and Functionalization of Monolayer InSe by Physisorption of Small Molecules for Gas Sensing. *J. Phys. Chem. C* **2017**, *121*, 10182−10193.

(27) Jin, H.; Li, J.; Dai, Y.; Wei, Y. Engineering the electronic and optoelectronic properties of InX (X = S, Se, Te) monolayers via strain. *Phys. Chem. Chem. Phys.* **2017**, *19*, 4855−4860.

(28) Hu, T.; Zhou, J.; Dong, J. Strain induced new phase and indirect-direct band gap transition of monolayer InSe. *Phys. Chem. Chem. Phys.* **2017**, *19*, 21722−21728.

(29) Ebrahim, S.; Raoof, M.; Ramadan, W.; Soliman, M. New self assembly single layer onto SiGe as a selective biosensor for single-strand DNA. *Microelectron. Eng.* **2016**, *160*, 87−93.

(30) Dey, A.; Das, D. Narrow band gap high conducting nc-$Si_{1-x}Ge_x$:H absorber layers for tandem structure nc-Si solar cells. *J. Alloys Compd.* **2019**, *806*, 1529−1535.

(31) Kennedy, N.; Duffy, R.; Mirabelli, G.; Eaton, L.; Petkov, N.; Holmes, J. D.; Hatem, C.; Walsh, L.; Long, B. Monolayer doping of silicon-germanium alloys: A balancing act between phosphorus incorporation and strain relaxation. *J. Appl. Phys.* **2019**, *126*, 025103.

(32) Pura, J. L.; Periwal, P.; Baron, T.; Jiménez, J. Growth dynamics of SiGe nanowires by the vapour-liquid-solid method and its impact on SiGe/Si axial heterojunction abruptness. *Nanotechnology* **2018**, *29*, 355602.

(33) Şahin, H.; Cahangirov, S.; Topsakal, M.; Bekaroglu, E.; Akturk, E.; Senger, R. T.; Ciraci, S. Monolayer honeycomb structures of group-IV elements and III-V binary compounds: First-principles calculations. *Phys. Rev. B: Condens. Matter Mater. Phys.* **2009**, *80*, 155453.

(34) Zhou, H.; Zhao, M.; Zhang, X.; Dong, W.; Wang, X.; Bu, H.; Wang, A. First-principles prediction of a new Dirac-fermion material: silicon germanide single layer. *J. Phys.: Condens. Matter* **2013**, *25*, 395501.

(35) Zhang, W. X.; Wang, Y. B.; Zhao, P.; He, C. Tuning the electronic and magnetic properties of graphene-like SiGe hybrid nanosheets by surface functionalization. *Phys. Chem. Chem. Phys.* **2016**, *18*, 26205−26212.

(36) Chen, X.; Sun, X.; Yang, D. G.; Meng, R.; Tan, C.; Yang, Q.; Liang, Q.; Jiang, J. SiGe/h-BN heterostructure with inspired electronic and optical properties: a first-principles study. *J. Mater. Chem. C* **2016**, *4*, 10082−10089.

(37) Blöchl, P. E. Projector augmented-wave method. Efficient iterative schemes for ab initio total-energy calculations using a plane-wave basis set. *Phys. Rev. B: Condens. Matter Mater. Phys.* **1994**, *50*, 17953.

(38) Kresse, G.; Hafner, J. Ab initio molecular dynamics for liquid metals. Generalized Gradient Approximation Made Simple. *Phys. Rev. B: Condens. Matter Mater. Phys.* **1993**, *47*, 558.

(39) Kresse, G.; Furthmüller, J. Efficient iterative schemes for ab initio total-energy calculations using a plane-wave basis set. *Phys. Rev. B: Condens. Matter Mater. Phys.* **1996**, *54*, 11169.

(40) Perdew, J. P.; Burke, K.; Ernzerhof, M. Generalized Gradient Approximation Made Simple. *Phys. Rev. Lett.* **1996**, *77*, 3865.

(41) Heyd, J.; Scuseria, G. E.; Ernzerhof, M. Erratum: "Hybrid functionals based on a screened Coulomb potential" [J. Chem. Phys. 118, 8207 (2003)]. *J. Chem. Phys.* **2006**, *124*, 219906.

(42) Henkelman, G.; Arnaldsson, A.; Jónsson, H. A fast and robust algorithm for Bader decomposition of charge density. *Comput. Mater. Sci.* **2006**, *36*, 354−360.

(43) Grimme, S.; Ehrlich, S.; Goerigk, L. Effect of the damping function in dispersion corrected density functional theory. *J. Comput. Chem.* **2011**, *32*, 1456−1465.

(44) Alfè, D. PHON: A program to calculate phonons using the small displacement method. *Comput. Phys. Commun.* **2009**, *180*, 2622−2633.

(45) Hamer, M. J.; Zultak, J.; Tyurnina, A. V.; Zólyomi, V.; Terry, D.; Barinov, A.; Garner, A.; Donoghue, J.; Rooney, A. P.; Kandyba, V.; Giampietri, A.; Graham, A.; Teutsch, N.; Xia, X.; Koperski, M.; Haigh, S. J.; Fal'ko, V. I.; Gorbachev, R. V.; Wilson, N. R. Indirect to Direct Gap Crossover in Two-Dimensional InSe Revealed by Angle-Resolved Photoemission Spectroscopy. *ACS Nano* **2019**, *13*, 2136−2142.

(46) Yagmurcukardes, M.; Senger, R. T.; Peeters, F. M.; Sahin, H. Mechanical properties of single layer GaS and GaSe crystals. *Phys. Rev. B* **2016**, *94*, 245407.

(47) Amin, B.; Singh, N.; Schwingenschlogl, U. Heterostructures of transition metal dichalcogenides. *Phys. Rev. B: Condens. Matter Mater. Phys.* **2015**, *92*, 075439.

(48) Fan, Y.; Liu, X.; Wang, J.; Ai, H.; Zhao, M. Silicene and germanene on InSe substrates: structures and tunable electronic properties. *Phys. Chem. Chem. Phys.* **2018**, *20*, 11369−11377.

(49) Liu, K.; Yan, Q.; Chen, M.; Fan, W.; Sun, Y.; Suh, J.; Fu, D.; Lee, S.; Zhou, J.; Tongay, S.; Ji, J.; Neaton, J. B.; Wu, J. Elastic Properties of Chemical-Vapor-Deposited Monolayer MoS_2, WS_2, and Their Bilayer Heterostructures. *Nano Lett.* **2014**, *14*, 5097−5103.

DOI: 10.1021/acs.jpcc.9b06404
J. Phys. Chem. C 2019, 123, 31232−31237